

Probing the sensitivity of the total nucleus-nucleus reaction cross section at intermediate energies to medium effects and isospin asymmetries.

Francesca Sammarruca and Larz White

*Physics Department, University of Idaho, Moscow, ID 83844-0903, U.S.A **

(Dated: November 25, 2021)

This paper presents reaction cross section predictions. These predictions are the result of a continuous pipeline which originates from a microscopic nuclear interaction. Density parameters and effective nucleon-nucleon cross sections (both involved in the reaction calculations) are by-products of the same equation of state. First, we perform tests of sensitivity to medium effects using reactions involving ^{208}Pb , a stable but weakly isospin-asymmetric nucleus. We also show predictions for collisions of some neutron-rich isotopes of Calcium and Argon. We observe significant sensitivity of the reaction cross section to medium effects but very weak sensitivity to inclusion of isospin asymmetry in the effective nucleon-nucleon cross sections.

I. INTRODUCTION

Collisions of neutron-rich ions can be exploited to investigate isospin asymmetries of nuclear matter. This is a topic of great current interest which impacts both terrestrial nuclear physics and the physics of neutron stars. The on-going and up-coming experimental programs using radioactive nuclear beams are expected to improve our knowledge of nuclear properties away from the stability line, making predictions of neutron-rich systems especially interesting and timely.

Interaction cross section measurements can provide valuable information on the structure of exotic nuclei. In this paper, we will be concerned specifically with the nucleus-nucleus total reaction cross section and its sensitivity to medium effects and to the inclusion of isospin asymmetries. By isospin asymmetries we mean: 1) Separating neutron and proton densities in the target and projectile nuclei, as opposed to just considering total *nucleon* densities (something which is often done for mildly isospin-asymmetric nuclei); and 2) *Medium-induced* differences between collisions of different types of nucleons in the presence of unequal concentrations of protons and neutrons. (Notice that we are not referring to the well-known differences between pp/nn and np cross sections.) Intermediate energies are best for our purpose, as both the model approximations we apply and the expectation of sensitivity to medium effects are reasonably justified.

Isospin-dependent dynamics can be studied through a variety of reactions/phenomena related to the transport of protons and neutrons. A review of isospin effects in heavy-ion reactions which may be particularly suitable to probe the nuclear symmetry energy can be found in Ref. [1]. Furthermore, fusion dynamics in heavy-ion collisions close to the Coulomb barrier is sensitive to the incident energy and the neutron-to-proton ratio in the neck region of the colliding systems [2]. More recently, isospin and symmetry energy effects on the competition between fusion and break-up reactions in low-energy (about 10A MeV) heavy-ion collisions have been studied within a stochastic mean-field approach [3]. When exotic beams are employed, these mechanisms are expected to be sensitive to the isovector part of the nuclear potential, thus yielding information on the symmetry energy. In passing, we note that the mean field used in calculations such as those from Ref. [3] is often derived from phenomenological forces. We hope that these very comprehensive reaction studies will consider including predictions from microscopic many-body calculations as part of their input.

Although a rather global observable as compared to the potentially more “selective” mechanisms mentioned above, the reaction cross section has the potential to reveal sensitivities to effects induced by isospin asymmetry in the medium, particularly when written in such a way as to discriminate between protons and neutrons (see Section **IIA**, Eq. (8)). It is then interesting to explore to which extent this is true.

This paper is organized as follows. In Section **II**, we review some formal aspects of reaction cross section calculations (within the optical limit of the Glauber model (GM) [4]) and describe the main input, namely the nucleon-nucleon (NN) collisions and the nuclear densities. In our case, both of these ingredients are obtained from, or are closely related to, our microscopic equation of state (EoS), making all aspects of our calculation internally consistent with

*Electronic address: fsmarr@uidaho.edu

one underlying nuclear interaction. We will discuss how medium effects and isospin asymmetries are introduced in the various elements of our calculation. Within Section II, we will look at the reaction cross section for collisions of stable nuclei and perform some sensitivity studies. We have chosen collisions of ^{40}Ca on ^{208}Pb as our initial ‘‘laboratory’’. Although not an exotic one, ^{208}Pb is an interesting nucleus to consider, since very accurate measurements of its neutron skin are expected to come from the electroweak physics program at the Jefferson Laboratory. (To the best of our knowledge, such value is not yet available, but we understand that the JLAB target uncertainty should be very small.)

Several authors have confronted reaction cross sections with neutron-rich isotopes (see, for instance, Ref. [5] for Carbon isotopes incident on a proton). In Section III we will look at some reaction cross section data for collisions involving neutron-rich isotopes of Calcium and Argon at energy/nucleon between 50 and 70 MeV [6]. For that purpose, we need neutron and proton densities for the nuclides under consideration. Again, we obtain density distributions from our equation of state and then move to predictions of reaction cross sections.

Our conclusions and future outlook are summarized in Section IV.

II. THE REACTION CROSS SECTION

A. Review of some formal aspects

We operate within the optical limit of the Glauber model [4]. The reaction cross section is written, in terms of the impact parameter b , as

$$\sigma_R = 2\pi \int_0^\infty (1 - T(b)) b db, \quad (1)$$

with $T(b)$ the *nuclear transparency*, defined as

$$T(b) = e^{-\int P(b,z) dz}, \quad (2)$$

where the *thickness function* is given by [7]

$$P(b, z) dz = \bar{\sigma}(E) \rho_T(b, z) \rho_P(b, z) dz. \quad (3)$$

Namely, the thickness function is the product of the averaged NN cross section and the overlap integral of the target and projectile densities, ρ_T and ρ_P . The averaged NN cross section is defined as

$$\bar{\sigma}(E) = \left(\frac{Z_T}{A_T} \frac{Z_P}{A_P} \right) \sigma_{pp}(E) + \left(\frac{N_T}{A_T} \frac{N_P}{A_P} \right) \sigma_{nn}(E) + \left(\frac{Z_T}{A_T} \frac{N_P}{A_P} + \frac{N_T}{A_T} \frac{Z_P}{A_P} \right) \sigma_{np}(E), \quad (4)$$

where $Z_{T(P)}$, $N_{T(P)}$, and $A_{T(P)}$ are the proton, neutron, and mass numbers of the target(projectile) nucleus, and $\sigma_{ii}(\sigma_{ij})$ are the elementary cross sections for scattering of identical(non-identical) nucleons.

More generally, and accounting for finite range nuclear interactions [8], one writes the transparency as

$$T(b) = \exp(-\bar{\sigma}(E) \int d^2 r_T \int d^2 r_P f(|\vec{r}_P - \vec{r}_T|) \rho_z^{(T)}(|\vec{r}_T|) \rho_z^{(P)}(|\vec{r}_P - \vec{b}|)), \quad (5)$$

where the z -integrated densities of the target and projectile nuclei are defined as

$$\rho_z^{(T)}(|\vec{r}_T|) = \int dz \rho^{(T)}((r_T^2 + z^2)^{1/2}) \quad (6)$$

and

$$\rho_z^{(P)}(|\vec{r}_P - \vec{b}|) = \int dz \rho^{(P)}((|\vec{r}_P - \vec{b}|^2 + z^2)^{1/2}). \quad (7)$$

In these expressions \vec{r}_P and \vec{r}_T are *transverse* coordinates, defined in the plane perpendicular to the beam axis.

Typically, the range function, $f(|\vec{r}_T - \vec{r}_P|)$, which is normalized to unity, is taken to be of Gaussian shape with an interaction range of about 0.6-1.0 fm [8]. Taking the range function to be a delta function, $\delta(\vec{r}_T - \vec{r}_P)$, amounts to adopting the zero-range approximation [7].

TABLE I: Point and charge r.m.s. radii (in units of fermi) predicted through our equation of state for ^{40}Ca and ^{208}Pb . The second and third column display the proton and neutron point radii. The fourth and fifth columns show the charge radius and its empirical value. The values in the second half of the Table are obtained ignoring differences between proton and neutron distributions. See text for details.

Nucleus	$\langle r_{r.m.s.} \rangle_p$	$\langle r_{r.m.s.} \rangle_n$	$\langle r_{r.m.s.} \rangle_{ch}$	$\langle r_{r.m.s.} \rangle_{ch}^{exp}$
^{208}Pb	5.39	5.56	5.45	5.52
^{40}Ca	3.43	3.39	3.52	3.48
^{208}Pb	5.45	5.45	5.51	5.52
^{40}Ca	3.41	3.41	3.50	3.48

The formulas above can be understood in terms of interaction probability between density elements in the target and projectile nuclei. Those density elements consist of “tubes” parallel to the beam axis (the z -axis) and whose position is specified by the vectors \vec{r}_T and \vec{r}_P . The use of z -integrated densities reduces an otherwise six-dimensional integral (similar to the double-folding of an effective nuclear interaction) to a four-dimensional one, which we calculate numerically. Alternatively, the integral can be rendered separable by Fourier transformation into momentum space [9].

Notice that, when properly discriminating between proton and neutron densities (beyond the Z/A and N/A factors which appear in Eq. (4)), the transparency function is written as

$$T(b) = \exp\left(- \int d^2r_T \int d^2r_P f(|\vec{r}_T - \vec{r}_P|) \sum_{i=n,p} \sum_{j=n,p} \sigma_{ij} \rho_{z,i}^{(T)}(\vec{r}_T) \rho_{z,j}^{(P)}(|\vec{r}_P - \vec{b}|)\right), \quad (8)$$

where the summations extend over neutron and proton densities of target and projectile. In the next section, we will discuss the inclusion of isospin asymmetry through the densities as well as the elementary cross sections.

A first-order Coulomb correction can be included by replacing the impact parameter with the (classical) distance of closest approach in the Coulomb field [10, 11]. That is, in Eq. (5) one replaces the impact parameter with

$$d = \frac{a}{2} + \sqrt{\left(\frac{a}{2}\right)^2 + b^2}, \quad (9)$$

where a is the distance of closest approach when $b = 0$. We apply such trajectory modification here.

Some comments are in place concerning the validity of the Glauber model in the energy range to be considered here, particularly the lower end of that range, which is 50 MeV/nucleon. The basic assumption of the Glauber model is the description of the relative motion of target and projectile in terms of straight trajectories. For low energy, the eikonal trajectories should be modified to account for both the Coulomb field and the nuclear field, with the nuclear field effect tending to move the reaction cross section closer to the Glauber model results. In Ref. [11], it is shown that the most significant effect at low and intermediate energies (from the Coulomb barrier to 50 times the Coulomb barrier) is the one due to the Coulomb field. In fact, close to the Coulomb barrier, the Coulomb-modified GM and the Coulomb plus nuclear modified GM appear indistinguishable. For a system such as $^{40}\text{Ca} + ^{208}\text{Pb}$, which we will confront next, 50 MeV/nucleon is about 10 times the Coulomb barrier (in terms of center-of-mass energy), and the results of Ref. [11] gives us some confidence that a (Coulomb-modified) GM is reasonably valid for our purposes. Kox *et al.* [12] included effects from the nuclear potential to compare modified GM predictions with their measurements (in the range of 10-300 MeV/nucleon). The potential was taken to be the real part of an optical potential extracted from analysis of elastic scattering data for similar reaction systems. They note that nuclear field effects can counterbalance the Coulomb repulsion in a significant way mostly for the lightest projectiles [13] (one reason why we prefer to work with medium-heavy nuclei).

Another mechanism that goes beyond the Glauber model is Pauli blocking, which is included in our in-medium NN cross sections (see below). Note, further, that our in-medium cross sections also contain nuclear mean field effects, being modified by the average nuclear matter potential.

Weighing all the considerations above, we remain well aware that several modifications of the Glauber model may be important at the lower energies, especially when a detailed comparison with the data is the main objective. Here, on the other hand, we focus mostly on exploring sensitivities.

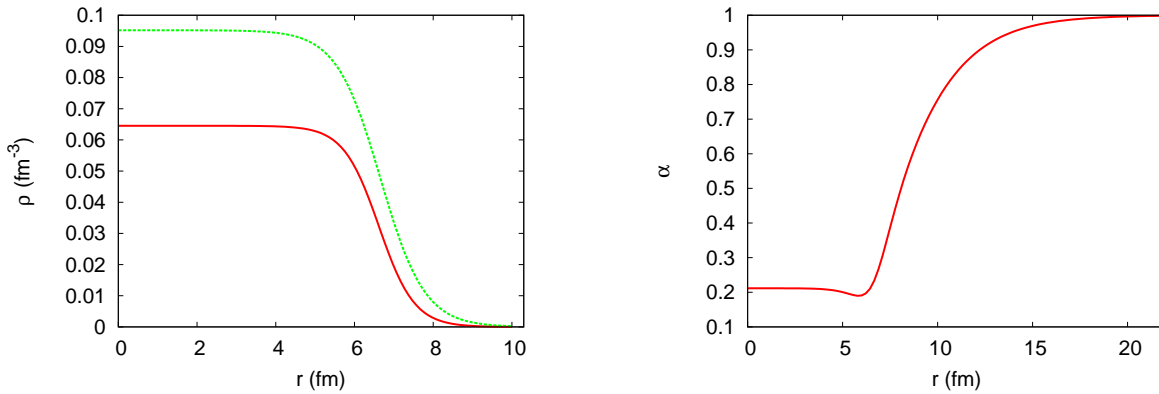


FIG. 1: (color online) Left frame: Two-parameter Fermi functions used to describe the neutron (dotted green curve) and the proton (solid red curve) densities in ^{208}Pb . Right frame: the neutron excess parameter, α , corresponding to the densities given on the left.

B. The proton and neutron densities

Our density functions are theoretical predictions obtained directly as point densities with the method described in Refs. [14, 15]. Our EoS is derived within the Dirac-Brueckner-Hartree-Fock (DBHF) approach to nuclear matter together with the Bonn B NN potential [16]. We write an energy functional based on the mass formula, where the “volume term” contains the energy per particle as a function of density (namely, the EoS). The density functions that appear in the various integral terms of the mass formula are parametrized as two-parameter Fermi functions (best suited for medium to heavy nuclei),

$$\rho(r) = \frac{\rho_0}{1 + e^{(r-r_0)/c}}, \quad (10)$$

and the parameters r_0 and c are then determined from energy minimization. In this way, when the asymmetric matter EoS is used in the mass formula, we can extract parameters of both neutron and proton densities, as we have done previously for the purpose of predicting the neutron skin of ^{208}Pb [14, 15]. The proton and neutron densities in ^{208}Pb thus calculated are shown in the left frame of Fig. 1. The corresponding neutron skin is equal to 0.169 fm. On the right side of the same figure we show the predicted isospin asymmetry parameter in ^{208}Pb , $\alpha = (\rho_n - \rho_p)/(\rho_n + \rho_p)$, as a function of the radial coordinate from the center of the nucleus. The asymmetry parameter is close to 0.2 up to a radial distance of about 5 fm, but it can reach values up to 0.7 in the skin.

In Table I, we show our predicted r.m.s. radii for ^{208}Pb and ^{40}Ca . The values displayed in the upper half of the Table are obtained with our asymmetric matter EoS. For ^{40}Ca our calculation predicts a small but negative skin, an indication that the neutrons form a slightly more compact system than the protons. The values in the lower half of the Table are obtained imposing that the density profile is the same for neutrons and protons. Consistent with that assumption (which clearly results into a neutron skin equal to zero), we use the symmetric matter equation of state in the energy functional when searching for those parameters.

We now move to a discussion of Fig. 2. The solid line shows the predictions we obtain ignoring differences between proton and neutron density distributions, which are then scaled with Z/A and N/A factors as in Eq. (4), whereas the dotted line is obtained with the neutron and proton densities shown in Fig. 1. Typical differences between the solid and the dotted lines amount to about 2-3%. The dash-dotted line in Fig. 2 is obtained using neutron and proton density functions derived from a different EoS, as we explain next. In Ref. [14] we compared a family of EoS based on the Brueckner-Hartree-Fock approach implemented with three-body forces (TBF), on the one hand, and our DBHF-based EoS, on the other. In particular, we compared predictions of the symmetry pressure, proportional to the derivative of the symmetry energy, and the (strongly correlated) neutron skin in ^{208}Pb . The EoS employed for the dash-dotted line in Fig. 2 is the one referred to as U1X in Ref. [14], which utilizes the Argonne V18 potential [17] and the phenomenological Urbana TBF [18]. It is considerably more repulsive than our EoS and predicts a larger neutron skin for ^{208}Pb . According to our calculation, that value is 0.226 fm *vs* 0.169 fm (our prediction), a 33% increase. Nevertheless, the (EoS-induced) differences between the dotted and the dash-dotted lines in Fig. 2 are of the order of 4-5%, implying that data precision at this level would be necessary to distinguish between the two EoS applied for this test. On the other hand, we must keep in mind that in a different system, such as a nucleus with a very large skin or halo, the model dependence displayed in Fig. 2 may be more significant and may have the potential to help discriminating among different EoS.

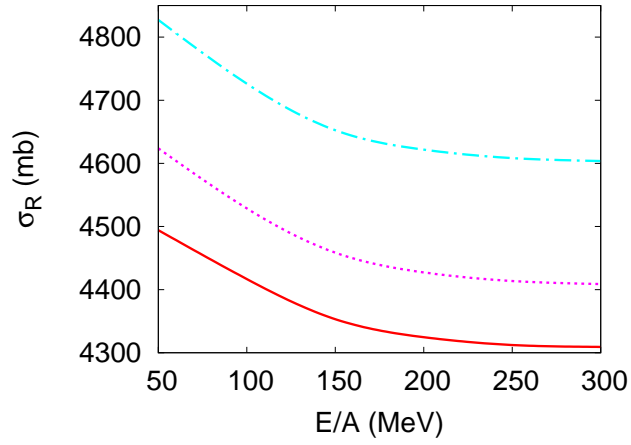


FIG. 2: (color online) Total reaction cross section for ^{40}Ca on ^{208}Pb as a function of the energy/nucleon. The dotted (pink) line is obtained with proton and neutron densities leading to the predictions in the upper half of Table I, whereas the solid (red) curve corresponds to the predictions in the lower half of Table I. The dash-dotted (blue) line is obtained with density functions derived from a different EoS, as explained in the text. Free-space NN cross sections are employed.

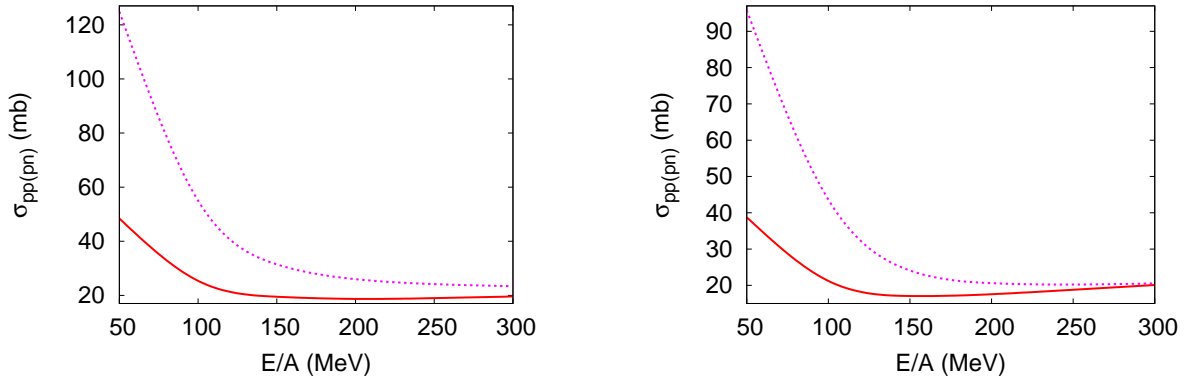


FIG. 3: (color online) Our in-medium NN cross sections in symmetric matter with a Fermi momentum equal to 1.1 fm^{-1} (left side) and 1.3 fm^{-1} (right side). Dotted (pink) line: np ; solid (red) line: identical nucleons.

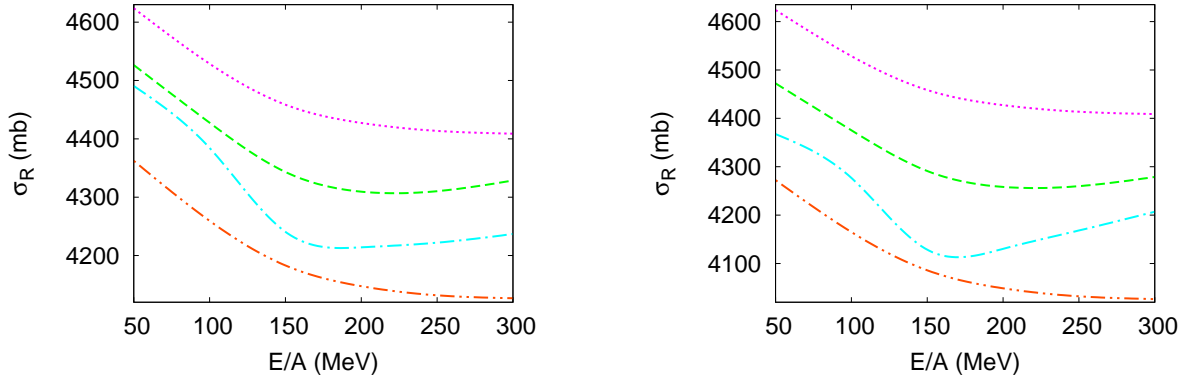


FIG. 4: (color online) Total reaction cross section for ^{40}Ca on ^{208}Pb as a function of the energy/nucleon. The dotted (pink) line employs free-space NN cross sections. The other three predictions make use of different models for the calculation of medium effects, as detailed in the text. An average density equal to 0.089 fm^{-3} (0.148 fm^{-3}) is assumed in the left (right) panel.

C. The nucleon-nucleon cross sections: medium and isospin asymmetry effects

In previous papers [19, 20] we have confronted the issue of microscopic in-medium NN cross sections. We discussed how the very definition of in-medium cross sections can be ambiguous, because the scenario of two particles scattering in the medium requires, at the very least, kinematical choices that are not unique. Furthermore, how to properly include Pauli blocking has to be considered carefully [19, 21].

The effective NN cross sections we apply in this work are shown in Fig. 3 at two different densities of symmetric matter. They include modifications of the microscopic G-matrix through Pauli blocking of the intermediate states and modifications of the single-particle energy by the nuclear matter mean field, parametrized through the nucleon effective mass. The latter is a direct by-product of the EoS calculation.

In a much simpler approach, one makes the assumption that the transition matrix in the medium is approximately the same as the one in vacuum and that medium effects come in only through the use of effective masses in the phase space factor [22–24]. In that case, in-medium cross sections are scaled (relative to their value in vacuum) as the square of the ratio of the (reduced) masses. Namely,

$$\sigma_{NN}^*/\sigma_{NN} = (\mu_{NN}^*/\mu_{NN})^2, \quad (11)$$

where σ^* stands for the cross section at non-zero density. In summary, the issue of how to define and calculate microscopic in-medium NN cross sections remains an interesting and unsettled one.

We will now proceed to explore sensitivity of the reaction cross section with respect to the model adopted to describe medium effects on the NN cross sections.

In Fig. 4, we show again the reaction cross section for ^{40}Ca on ^{208}Pb as a function of the energy/nucleon. The dotted (pink) line is the same as the dotted line in Fig. 2 and employs free-space NN cross sections. All other predictions include medium effects calculated in *symmetric* nuclear matter at some average density of 0.089 fm^{-3} (left frame) and 0.148 fm^{-3} (right frame). The dash-dotted (blue) line employs our microscopic in-medium NN cross sections as shown in Fig. 3 (method I). As mentioned above, they are the result of DBHF G-matrix calculations which include Pauli blocking of the intermediate states and (self-consistent) modification of the nucleon mass through dispersive effects on the single-particle energy. The predictions shown by the dashed (green) line make use of in-medium NN cross sections derived from the phenomenological formula of Ref. [25] (method II). The latter combines the energy dependence of free space cross sections with the density dependence from the microscopic model of Refs. [26, 27], although we found that the agreement with the latter is only approximate. At this point we note that the calculations of Refs. [26, 27] are also based on the DBHF approach to nuclear matter, but medium effects are applied to the (real) K-matrix while we work with the (complex) G-matrix. We found that it is important to do so (even below the inelastic threshold, where of course the two methods would yield identical predictions in free space), because application of Pauli blocking, by removing energetically open channels, amounts to violation of free-space unitarity. On the other hand, calculation of NN phase shifts from the real K-matrix imposes free-space unitarity. We believe this is the reason why there is a non-negligible difference between our predictions and those of Refs.[26, 27]. Finally, the dash-double-dotted (orange) line is obtained using NN cross sections from the mass scaling formula, Eq. (11), where we have used our dynamically generated effective masses (method III).

The strongest medium effects are seen with the simplest approach, namely method III. Also, medium effects are non-linear with density. It is interesting to observe that the predictions obtained with the microscopic NN cross sections show more structure in their energy dependence. The slow rise at the higher energies (see left panel of Fig. 4) is very similar to the one displayed by the dashed line (we recall that the latter uses NN in-medium cross sections which, to a certain extent, simulate a microscopic DBHF model). Such rise is more pronounced at the higher density (see right side of the figure) and is mostly due to enhancement of the in-medium pp cross sections, a phenomenon that has been observed by other authors as well [20, 26, 27].

The largest differences seen in Fig. 4 (relative to the free-space results) amount to about 6% at the lower density (left frame) and approximately 8-9% at the higher density (right frame). We conclude that medium effects can be significant. (Of course the densities involved in a particular collision are functions of space, and so should be the NN in-medium cross sections. With our sensitivity tests we have certainly covered a typical density range probed by these reactions.)

We now move on to effects from neutron/proton asymmetry in the NN collisions. Our DBHF calculation of the asymmetric matter EoS and related quantities (such as the symmetry potential and the effective masses for neutrons and protons) is described in details in Ref. [14]. For a given total density, we allow the population of one nucleon species to increase. The presence of two different Fermi levels results into self-consistent potentials, and thus effective masses, which are different for neutrons and protons. As a consequence, in-medium cross sections for identical nucleons (pp or nn) are different from each other. (It should be clear that we are referring to strong interaction cross sections and to differences that are unrelated to charge.) We also explored isospin effects on the in-medium pn cross section

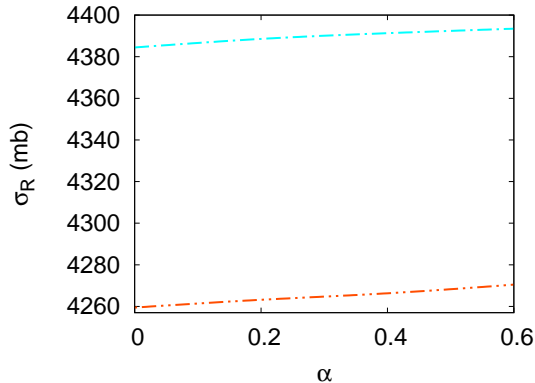


FIG. 5: (color online) Total reaction cross section for ^{40}Ca on ^{208}Pb at $E/A=100$ MeV. The effective NN cross sections are calculated with method I (dash-dotted, blue) and method III (dash-double-dotted, orange), assuming an average density of 0.068 fm^{-3} and including isospin asymmetry as explained in the text.

and found them entirely negligible, due to the fact that the two different nucleon species are oppositely impacted by those effects as the population of one species increases.

To include isospin asymmetry within method III, we simply apply the appropriate effective masses (this time, different for protons and neutrons) in Eq. (11). (The formula previously referred to as “method II” does not incorporate this kind of isospin degree of freedom and thus is not included in the discussion of Fig. 5.)

These NN cross sections, now energy, density, and α dependent, are then inserted in Eq. (8). Figure 5 shows the total reaction cross sections at 100 MeV (in terms of E/A) and a fixed moderate density ($\rho=0.068\text{ fm}^{-3}$) as a function of the neutron excess parameter as defined in Section II B. More precisely, each value of α represents some average neutron/proton asymmetry that is being attributed to the colliding system for the purpose of sensitivity testing. Clearly, the slope of the two lines shown in the figure is insignificant, especially compared to the differences between the two sets of predictions. Thus, sensitivity to isospin dependence of the NN cross sections can be disregarded in this observable, an observation that may be of practical relevance.

III. REACTION CROSS SECTION WITH NEUTRON-RICH ISOTOPES

In this section, we will consider reactions with some neutron-rich isotopes of Calcium and Argon. This choice is motivated by the following. Neutron-rich Calcium isotopes have been studied in Ref. [28] within the relativistic Hartree (RH) theory, a very popular, although not microscopic, approach to describe nuclear properties. Neutron and proton radii, charge radii, and binding energies are given in that work for several parameter sets of the model. At the same time, reaction cross section measurements exist for some of those isotopes. This gives us some reference point to compare our predictions with as we move continuously from our nuclear density predictions to the reaction cross section calculations.

As before, our nuclear densities are extracted assuming Thomas-Fermi functions as in Eq. (9) together with our microscopic equation of state. A comparison with RH predictions is shown in Table II. There, for given Z and A , the first set of predictions is from our work whereas the second is from Ref. [28], specifically the parameter set referred to as “HS” [29], with the exception of ^{64}Ca , for which results were given only with the set “TS” [30]. (Notice that the TS predictions, shown for the last isotope, are generally smaller than the HS ones, which, on the other hand, are very similar to those from models that include non-linearities in the σ potentials [31].)

First, we note that, overall, the predictions are in reasonable agreement with each other. Considering that empirical values for nuclear matter saturation properties and the symmetry energy are used to determine the parameters in the Hartree theory, it appears that our microscopic EoS has reasonable predictive power, even when used in a simple liquid drop model.

The average isospin asymmetry parameter for the isotopes shown in the Table changes from 0 to 0.375, the last being considerably larger than in lead. Generally, the proton radius changes only little with increasing neutron population. For $A=40$, the neutron skin is very small and negative, as discussed previously. Beyond $A=48$, in our predictions the skin increases continuously with increasing N , from -0.046 fm to 0.553 fm . Na isotopes with A from 20 to 32 were studied in Ref. [33] (also using parametrizations as in Eq. (10)) and a monotonic increase in the neutron skin thickness was observed as well.

The data shown in Fig. 6 are part of measurements taken at the National Superconducting Cyclotron Laboratory

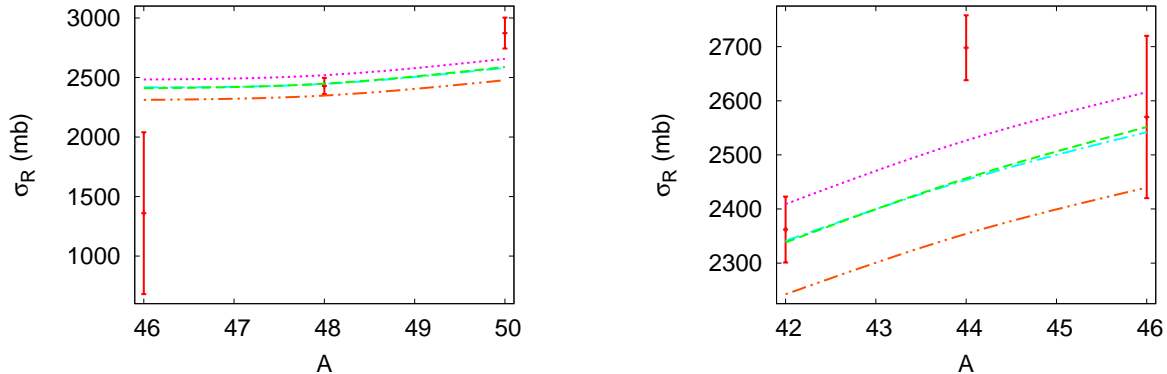


FIG. 6: (color online) Total reaction cross sections as a function of the mass number of Calcium isotopes (left frame) and Argon isotopes (right frame). Dotted (pink) line: free-space NN cross sections; Dash-dotted (blue) line: in-medium cross sections from method I; dashed (green) line: in-medium cross sections from method II; dash-double-dotted (orange) line: in-medium cross sections from method III. Data from Ref. [6].

TABLE II: Some nuclear properties for the neutron-rich isotopes considered in this work. For each set of (Z,A) values, the first row contains predictions from this work, whereas the second is from Ref. [28]. The items shown in the table are the (point) neutron, (point) proton, and charge r.m.s. radii, and the energy per particle.

Z	A	$r_p(fm)$	$r_n(fm)$	$r_{ch}(fm)$	e/A (MeV)
20	40	3.433	3.387	3.525	-7.68
		3.387	3.332	3.483	-6.51
20	46	3.448	3.555	3.539	-7.91
		3.374	3.535	3.470	-6.76
20	48	3.446	3.545	3.538	-7.82
		3.375	3.588	3.471	-6.86
20	50	3.479	3.702	3.571	-7.78
		3.394	3.733	3.490	-6.72
20	52	3.506	3.790	3.596	-7.67
		3.414	3.854	3.508	-6.61
20	54	3.535	3.845	3.625	-7.53
		3.440	3.929	3.534	-6.42
20	60	3.616	4.080	3.704	-7.04
		3.514	4.144	3.606	-6.05
20	64	3.663	4.216	3.750	-6.67
		3.348	3.878	3.445	-7.12

[6] at energies/particle between 50 and 70 MeV (depending on the isotope), where silicon detectors were also utilized as targets. The predictions we show next are obtained assuming a target of ^{28}Si and some of the different Calcium and Argon isotopes as projectiles. (We are limiting our considerations to isotopes with even A and Z , to maximize the validity of the spherical symmetry assumption.) At this point we neglect isospin dependence of the NN cross sections because of the observations made at the end of the previous section.

Figure 6 shows reaction cross section predictions and data for Calcium isotopes (left frame) and Argon (right frame). The various curves are obtained with: free-space NN cross sections (pink, dotted); medium modified NN cross sections as in method I (dash-dotted, blue); medium modified NN cross sections as in method II (dashed, green); medium modified NN cross sections as in method III (dash-double-dotted, orange). A moderate average density of 0.068 fm^{-3} (between 1/2 and 1/3 of normal nuclear density) is assumed.

Although they cannot be discerned at the level of precision of these data, medium effects can be significant. It is important for theorists to agree on accurate calculations of medium effects before other issues can be addressed reliably (such as the nature of “exotic” nuclear matter distribution).

IV. CONCLUSIONS

In closing, we stress that one of the main features of our work is a seamless and parameter-free pipeline (from the effective NN interaction to the EoS, to nuclear densities, to in-medium NN cross sections, to reaction cross sections) originating from one single realistic NN potential [16]. For the purpose of this sensitivity study, we adopted a reaction model that has been traditionally used due to its convenience and simplicity. In the near future, we plan to remove some of the approximations inherent to the optical limit of the Glauber model [34].

We have performed sensitivity tests with the total reaction cross section involving stable (although mildly isospin asymmetric) nuclei, such as ^{208}Pb . This observable has the potential to discriminate among different EoS yielding different predictions for the neutron distribution of neutron-rich nuclei.

We explored the impact of applying medium effects on the NN cross sections. Taking as a reference point standard data sets with stable nuclei such as those by Kox *et al.* [12], we see that error bars can be as small as 6-7% and occasionally as large as 20% or more. Overall, this level of precision would make it difficult to resolve the model dependence of the reaction cross section with respect to medium effects. Nevertheless, theorists should feel encouraged to find better agreement concerning the best definition and calculation of effective in-medium NN cross sections.

In a problem as complex as the one of heavy-ion reactions, where several ingredients are necessary and none of them is free of uncertainty, one has to be very selective of the appropriate “laboratory”. Reactions with exotic nuclei at high energy (as those measured, for instance, in Ref. [33] at 950A MeV), where medium effects can be expected to be negligible, are best suited to probe matter distribution beyond stability. Once reliable information on the structure is available, that information can be used in calculations of lower-energy reactions where the focus can be placed on the density-dependence of the nuclear interaction.

As noted in the Introduction, the isospin degree of freedom plays an important role in heavy-ion collisions, especially the transport of neutrons and protons. It was found [24] that in-medium NN cross sections have significant influence on the isospin transport and the nucleon transverse flow at intermediate energy. Although here we are not dealing with a transport model, the transparency, written as in Eq. (8), allows for a natural separation of the nn , pp , and np cross sections. Sensitivity to such separation, if any, would result from different probabilities (of the different types of collisions) in the overlap region of isospin asymmetric colliding ions. We explored whether such differences can be detected by the reaction cross section and concluded that they cannot.

Ultimately, the possibility of exploiting this and other reaction observables to constrain nuclear properties and/or medium modifications of the nuclear force rests on the availability of large systematics and good-precision data. These are precisely among the major goals of upcoming experimental efforts in nuclear physics.

Acknowledgments

Support from the U.S. Department of Energy under Grant No. DE-FG02-03ER41270 is acknowledged.

-
- [1] Bao-An Li, Lie-Wen Chen, and Che Ming Ko, Phys. Rep. **464**, 113 (2008).
 - [2] Zhao-Qing Feng and Gen-Ming Jin, Phys. Rev. C **80**, 037601 (2009).
 - [3] C. Rizzo, V. Baran, M. Colonna, A. Corsi, and M. Di Toro, Phys. Rev. C **83**, 014604 (2011).
 - [4] R.J. Glauber, *Lectures on Theoretical Physics* (Interscience, New York, 1959) Vol.I.
 - [5] B. Abu-Ibrahim, W. Horiuchi, A. Kohama, and Y. Suzuki, Phys. Rev. C **77**, 034607 (2008).
 - [6] I. Licot *et al.*, Phys. Rev. C **56**, 250 (1997).
 - [7] P. Karol, Phys. Rev. C **11**, 1203 (1975).
 - [8] G.F. Bertsch, B.A. Brown, and H. Sagawa, Phys. Rev. C **39**, 1154 (1989).
 - [9] G.R. Satchler and W.G. Love, Phys. Rep. **55**, 183 (1979).
 - [10] R.M. De Vries and J.C. Peng, Phys. Rev. C **22**, 1055 (1980).
 - [11] Prashant Shukla, Phys. Rev. C **67**, 054607 (2003).
 - [12] S. Kox *et al.*, Phys. Rev. C **35**, 1678 (1987).
 - [13] D.M. Brink and G.R. Satchler, J. Phys. G **7**, 43 (1981).
 - [14] F. Sammarruca, Int. J. Mod. Phys. E, **19**, 1259 (2010).
 - [15] F. Sammarruca and P. Liu, Phys. Rev. C **79**, 057301 (2009).
 - [16] R. Machleidt, Adv. Nucl. Phys. **19**, 189 (1989).
 - [17] R.B. Wiringa, V.G.J. Stoks, and R. Schiavilla, Phys. Rev. C **51**, 38 (1995).
 - [18] B.S. Pudliner, V.R. Pandharipande, J. Carlson, and R.B. Wiringa, Phys. Rev. Lett. **74**, 4396 (1995).
 - [19] F. Sammarruca and P. Krastev, Phys. Rev. C **73**, 014001 (2006).
 - [20] H.F. Zhang, Z.H. Li, U. Lombardo, P.Y. Luo, F. Sammarruca, and W. Zuo, Phys. Rev. C **76**, 054001 (2007).

- [21] C.A. Bertulani and C. De Conti, Phys. Rev. C **81**, 064603 (2010).
- [22] V. R. Pandharipande and S.C. Pieper, Phys. Rev. C **45**, 791 (1992).
- [23] D. Persram and C. Gale, Phys. Rev. C **65**, 064611 (2002).
- [24] Bao-An Li and Lie-Wen Chen, Phys. Rev. C **72**, 064611 (2005).
- [25] Cai Xiangzhou, Feng Jun, Shen Wenqing, Ma Yugang, Wang Jiansong, and Ye Wei, Phys. Rev. C **58**, 572 (1998).
- [26] G.Q. Li and R. Machleidt, Phys. Rev. C **48**, 1702 (1993).
- [27] G.Q. Li and R. Machleidt, Phys. Rev. C **49**, 566 (1994).
- [28] D. Hirata, H. Toki, T. Watabe, I. Tanihata, and B.V. Carlson, Phys. Rev. C **44**, 1467 (1991).
- [29] C.J. Horowitz and B. D. Serot, Nucl. Phys. **A368**, 503 (1981).
- [30] H. Toki, Y. Sugahara, D. Hirata, I. Tanihata, and B. Carlson, Nucl. Phys. **A524**, 633 (1991).
- [31] P. G. Reinhard, M. Rufa, J. Maruhn, W. Greiner, and J. Friedrich, Z. Phys. A **323**, 13 (1986).
- [32] I. Tanihata, Phys. Lett. B **289**, 261 (1992).
- [33] T. Suzuki *et al.*, Phys. Rev. Lett. **75**, 3241 (1995).
- [34] B. Abu-Ibrahim and Y. Suzuki, Phys. Rev. C **62**, 034608 (2000).